

# Rabi oscillations of a quantum dot exciton coupled to acoustic phonons: coherence and population readout: supplementary material

**DANIEL WIGGER<sup>1,\*</sup>, CHRISTIAN SCHNEIDER<sup>2</sup>, STEFAN GERHARDT<sup>2</sup>, MARTIN KAMP<sup>2</sup>, SVEN HÖFLING<sup>2,3</sup>, TILMANN KUHN<sup>1</sup>, AND JACEK KASPRZAK<sup>4,\*</sup>**

<sup>1</sup>*Institut für Festkörpertheorie, Universität Münster, Wilhelm-Klemm-Str. 10, 48149 Münster, Germany*

<sup>2</sup>*Technische Physik, Universität Würzburg, Am Hubland, 97074 Würzburg, Germany*

<sup>3</sup>*SUPA, School of Physics and Astronomy, University of St. Andrews, North Haugh, St. Andrews KY16 9SS, United Kingdom*

<sup>4</sup>*Univ. Grenoble Alpes, CNRS, Grenoble INP, Institut Néel, 38000 Grenoble, France*

\* e-mail: [d.wigger@www.de](mailto:d.wigger@www.de), [jacek.kasprzak@neel.cnrs.fr](mailto:jacek.kasprzak@neel.cnrs.fr)

*Published 07 November 2018*

---

This document provides supplementary information to "Rabi oscillations of a quantum dot exciton coupled to acoustic phonons: coherence and population readout," <https://doi.org/10.1364/OPTICA.5.001442> on the following:

1. Spectra of the FWM signals and the laser pulses used in the two studied systems
  2. An additional temperature scan of photoluminescence spectra
  3. A demonstration of the vanishing Autler-Townes splitting for large pulse delays
  4. A brief discussion of the Purcell effect in the cavity system
  5. A calibration of the pulse areas in the two different photonic structures
  6. The missing time traces of the simulated entire four-wave mixing signals from the main text.
-

## 1. PULSE SPECTRA

Figure S1 shows four-wave mixing (FWM) spectral interferograms (orange and green) of the low-Q cavity system studied in the first part of the paper in (a) and the weakly coupled high-Q micro-pillar cavity system in (b), which is studied in the second part. Spectra of the respective reference pulses are shown in blue. The spectral width of the laser in (a) is matched to the cavity mode. Extra dips in the laser spectrum in (b) are caused by the strong water absorption within that spectral range. Spectral and temporal shapes of the excitation attaining the quantum dot layer in (b) is defined, not by the external excitation laser, but by the spectrally narrow cavity mode (around 50  $\mu\text{eV}$ ), governing the intracavity field and strongly spectrally filtering the impinging laser.

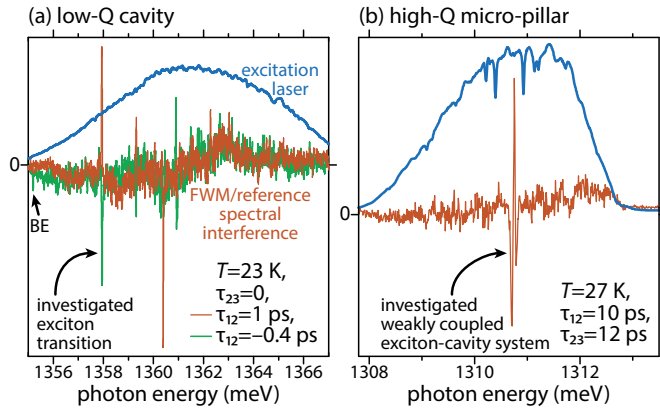


**Fig. S1.** Exemplary FWM spectral interferograms (orange and green traces) and spectra of the excitation laser (blue traces) measured on the low-Q planar micro-cavity (a) and high-Q micro-pillar (b). In (a) the exciton to biexciton transition is marked by BE.

## 2. PHOTOLUMINESCENCE SPECTRA

Figure S2 shows photoluminescence (PL) spectra of the quantum dot micro-pillar cavity system considered in the main text for varying temperature. With this we confirm that the exciton and the cavity mode do not form an anticrossing around their resonance. This proves that we are operating the system in the weak coupling regime. A corresponding temperature scan of the FWM signal is given in Fig. 2(b) in the main text.

## 3. AUTLER-TOWNES SPLITTING

In the main text in Figs. 3(c) and 3(d) we show two-pulse FWM spectra for different pulse areas  $\theta_1$  at the pulse delay  $\tau_{12} = 0$ . There we show that for large pulse areas the exciton transition splits into the two dressed states separated by the Autler-Townes (AT) splitting. In Figs. S3(a) and S3(b) corresponding spectra are shown for a delay of  $\tau_{12} = 30$  ps. In this case the overlap of the two driving laser pulses is small and the spectra do not show the AT splitting any longer. The simulation in (b) is in good agreement with the measurement in (a). This proves that the dressed states can only be resolved during the interaction with the first laser pulse. Following the signal intensity from small pulse areas to large ones we see that it forms two maxima. These are Rabi coherence rotations as we have discussed them in Ref. [1].

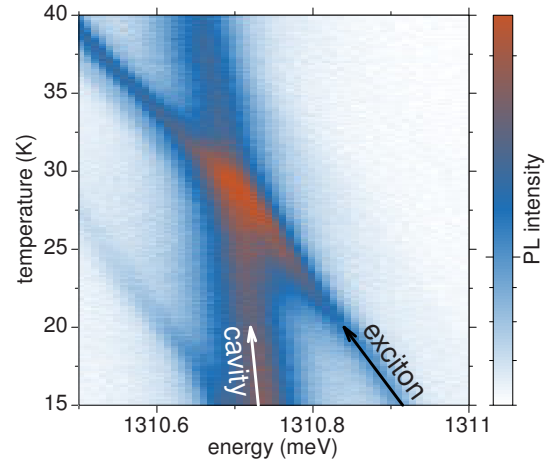


**Fig. S2.** Temperature scan of the photoluminescence spectra.

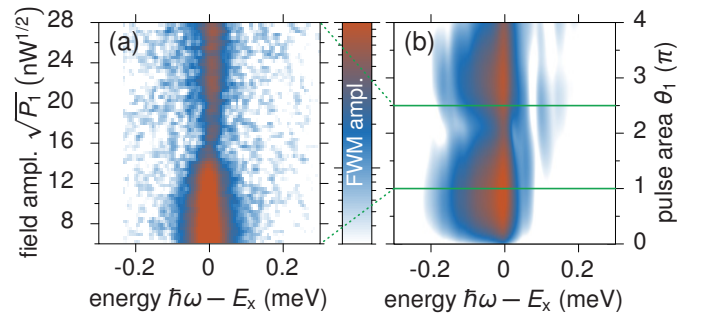


**Fig. S3.** Absence of the Autler-Townes splitting for large pulse delays. FWM spectra for different pulse areas at a delay of  $\tau_{12} = 30$  ps. (a) Measurement and (b) simulation.

## 4. PURCELL EFFECT

By measuring the three-pulse FWM signal in the micropillar-cavity system introduced in the main text, we can probe the radiative lifetime of the exciton state. In the main text we have shown that for small applied pulse areas the dynamics as a function of the delay  $\tau_{23}$  is governed by the radiative decay of the excited state population. The signal can be fitted by a single exponential. In Fig. S4(a) we show the measured FWM signal dynamics as colored solid lines. The corresponding exponential fits are given as green dashed lines. The temperature of the system increases from bottom to top trespassing the crossing in Fig. S2. Together with the detuning curves in Fig. S2 we can transfer the temperature of the system into a detuning between the cavity mode and the exciton transition. The fitted decay rates from Fig. S4(a) are plotted against the detuning in (b). We find the strongest radiative decay rate in the vicinity of the resonance, i.e., for vanishing detuning. For increasing negative and positive detunings the decay rate decreases rapidly. The reason for this result is the Purcell effect[2, 3] which gives rise to a decreasing radiative lifetime when the emitter is coupled stronger to the optical mode due to an increased density of photon states.

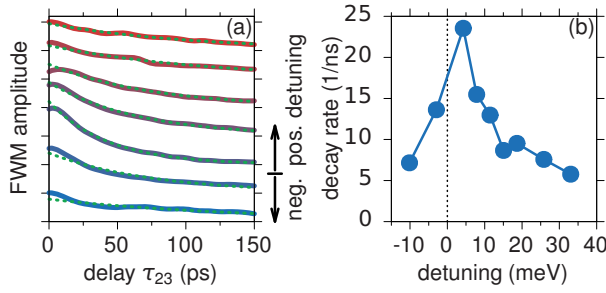


**Fig. S4.** Measurement of the Purcell effect. (a) Three-pulse FWM signal dynamics as a function of the delay  $\tau_{23}$ . The different temperatures, i.e., different detunings, increase from bottom to top. (b) Fitted decay rate as a function of the detuning between the cavity mode and the transition energy.

## 5. PULSE AREA CALIBRATION

In the main text we compare the dynamics of measured FWM signals for specific laser pulse powers with simulations, where certain pulse areas are considered to produce the best agreement with the experiment. In Fig. S5 we plot the fitted pulse areas  $\theta_i$  as a function of the square-root of the applied laser power  $\sqrt{P_i}$ , which is proportional to the field amplitude and therefore also to the pulse area in the experiment. Note, that for the results in Fig. 1 in the main text we used another QD sample than for the results in Figs. 4 and 5. For the uncertainties of the applied pulse power we assume 10% of  $P_i$  for the data from the micro-pillar cavity (Figs. 4 and 5) and 5% of  $P_i$  for the planar cavity (Fig. 1). The dotted lines in the plot are linear fits to the data points and serve as a guide to the eye. We find that the dependence between the field amplitudes in the experiment and the pulse areas in the theory follows the expected linear trend. The slope of the Fig. 4 and Fig. 5 data is similar, while the one for Fig. 2 is flatter. This is in line with the smaller Q-factor of the planar cavity used for Fig. 2.

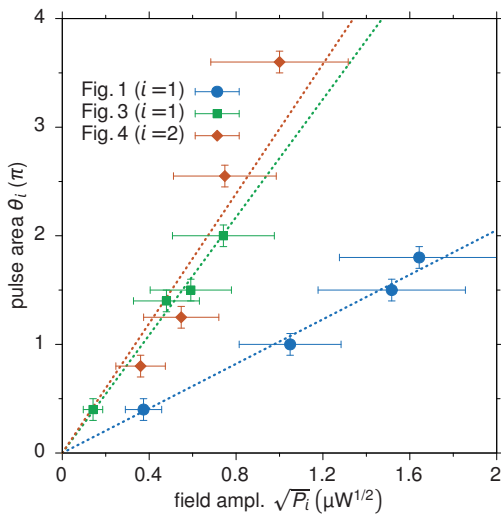


**Fig. S5.** Pulse areas calibration. Fitted pulse areas as function of applied field amplitude from the Figures in the main text as given in the plot.

## 6. COMPLEX FWM SIGNAL

Figure S6 shows the real and imaginary part of the FWM signals with the color coded delays  $\tau_{12}$  and  $\tau_{23}$ . In Fig. 6 in the main text we show the smallest and the largest considered pulse areas in the micro-pillar cavity system. Fig. S6 completes the considered pulse areas as it shows the remaining intermediate pulse areas from Figs. 4(b) and 5(d) from the main text. We see that by increasing the pulse areas an increasing number of loops appears in the plots. These loops represent the Rabi oscillations of the Bloch vector during the interaction with the laser pulses.

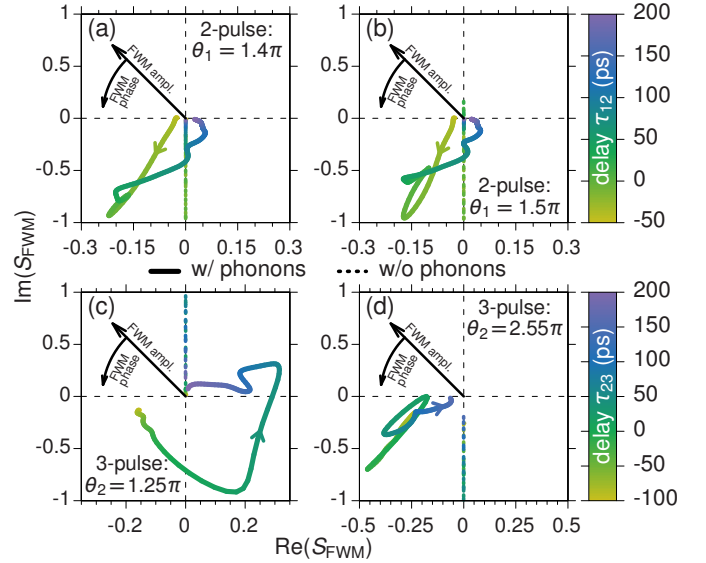


**Fig. S6.** Entire complex FWM signal. Real and imaginary part of the FWM signal  $S_{\text{FWM}}$ . The delays are color-coded, the dotted lines show simulations without phonon coupling and the solid lines with phonon coupling. (a, b) For two-pulse FWM. The corresponding dynamics of the FWM amplitude is given in Fig. 4(b) in the main text. (c, d) For three-pulse FWM. The corresponding dynamics of the FWM amplitude is given in Fig. 5(d) in the main text.

## REFERENCES

1. D. Wigger, Q. Mermillod, T. Jakubczyk, F. Fras, S. LeDenmat, D. E. Reiter, S. Höfling, M. Kamp, G. Nogues, C. Schneider, T. Kuhn, and J. Kapsrzak, "Exploring coherence of individual excitons in InAs quantum dots embedded in natural photonic defects: influence of the excitation intensity," *Phys. Rev. B* **96**, 165311 (2017).
2. E. M. Purcell, "Spontaneous emission probabilities at radio frequencies," *Phys. Rev.* **69**, 681 (1946).
3. J. M. Gerard and B. Gayral, "InAs quantum dots: artificial atoms for solid-state cavity-quantum electrodynamics," *Phys. E Low Dimens Syst Nanostruct* **9**, 131–139 (2001).